The Journal of Experimental Biology 215, 4115-4124

doi:10.1242/jeb.074484

RESEARCH ARTICLE

Transition from leg to wing forces during take-off in birds

Pauline Provini[1, 2,*], Bret W. Tobalske[3], Kristen E. Crandell[3] and Anick Abourachid[1]

[1]Muséum National d'Histoire Naturelle, EGB, UMR 7179, 55 rue Buffon, 75005 Paris, France, [2]Université Paris Descartes, 12 rue de l'Ecole de Médecine, 75270 Paris, France and [3]Field Research Station at Fort Missoula, Division of Biological Sciences, University of Montana, Missoula, MT 59812, USA

Author for correspondence (provini@mnhn.fr)

SUMMARY

Take-off mechanics are fundamental to the ecology and evolution of flying animals. Recent research has revealed that initial take-off velocity in birds is driven mostly by hindlimb forces. However, the contribution of the wings during the transition to air is unknown. To investigate this transition, we integrated measurements of both leg and wing forces during take-off and the first three wingbeats in zebra finch (*Taeniopygia guttata*, body mass 15 g, *N*=7) and diamond dove (*Geopelia cuneata*, body mass 50 g, *N*=3). We measured ground reaction forces produced by the hindlimbs using a perch mounted on a force plate, whole-body and wing kinematics using high-speed video, and aerodynamic forces using particle image velocimetry (PIV). Take-off performance was generally similar between species. When birds were perched, an acceleration peak produced by the legs contributed to 85±1% of the whole-body resultant acceleration in finch and 77±6% in dove. At lift-off, coincident with the start of the first downstroke, the percentage of hindlimb contribution to initial flight velocity was 93.6±0.6% in finch and 95.2±0.4% in dove. In finch, the first wingbeat produced 57.9±3.4% of the lift created during subsequent wingbeats compared with 62.5±2.2% in dove. Advance ratios were <0.5 in both species, even when taking self-convection of shed vortices into account, so it was likely that wing–wake interactions dominated aerodynamics during wingbeats 2 and 3. These results underscore the relatively low contribution of the wings to initial take-off, and reveal a novel transitional role for the first wingbeat in terms of force production.

Supplementary material available online at http://jeb.biologists.org/cgi/content/full/215/23/4115/DC1

Key words: zebra finch, *Taeniopygia guttata*, diamond dove, *Geopelia cuneata*, force, take-off, hindlimb, forelimb, velocity, acceleration, particle image velocimetry.

Received 28 April 2012; Accepted 13 August 2012

INTRODUCTION

Take-off initiates flight, and so plays a prominent role in the biology of flying birds. In living birds, take-off has an important function in predator–prey interactions, foraging, mate finding and many other ecologically pertinent tasks. In addition, take-off is also a key component of the evolutionary origin of flight. Indeed, for all three main hypotheses proposed for the origin of flight in birds, a transition between the substrate and the air is necessary before any kind of flight is accomplished, regardless of the substrate from which take-off occurs. These hypotheses include the traditional 'arboreal *versus* cursorial' origins (Ostrom, 1974; Padian, 1987) and an alternative hypothesis involving wing-assisted incline running (Dial, 2003). Thus, the debate about the origin of flight is closely linked to the ability to perform an effective take-off, and thus also to the contributions and coordination of the forelimbs and hindlimbs during this phase.

To date, only a small number of studies have focused on the mechanics of take-off in extant birds (Simpson, 1983; Heppner and Anderson, 1985; Dial and Biewener, 1993; Bonser and Rayner, 1996; Tobalske et al., 2004; Berg and Biewener, 2010) and even fewer have done so in the context of the origin of avian flight (Gatesy and Dial, 1993; Earls, 2000; Dial et al., 2008). Furthermore, the majority of studies that have explored take-off in extant birds have either emphasized aerial performance and consequently focused on the use of wings during take-off (Norberg and Norberg, 1971; Simpson, 1983; Heppner and Anderson, 1985; Tobalske and Dial, 2000; Askew et al., 2001; Berg and Biewener, 2010) or focused on the legs exclusively (Heppner and Anderson, 1985; Bonser and Rayner, 1996).

Only two studies have considered both locomotor systems during take-off (Earls, 2000; Tobalske et al., 2004). Kinematic and force plate analyses of birds with very different body shape and ecology (European starling *Sturnus vulgaris*, Japanese quail *Coturnix coturnix* and rufous hummingbird *Selasphorus rufus*) reveal that the hindlimbs rather than the forelimbs are the primary accelerators during take-off. Because these prior studies have shown that the hindlimbs dominate, our effort in the present study was to compare in greater detail the relative contributions of legs and wings to take-off performance. Here, we directly measured the contribution to force production of both legs and wings to gain an understanding of the interaction between legs and wings in reference to timing and aerodynamic forces.

We chose two species for our investigation: zebra finch (*Taeniopygia guttata*) and diamond dove (*Geopelia cuneata*) because of their dissimilar wing shapes and upstroke kinematics. Zebra finches are passerine birds with rounded wings of low aspect ratio. They present a highly flexed posture during upstroke, commonly termed a 'feathered' upstroke (Tobalske et al., 1999; Tobalske et al., 2003). In contrast, diamond doves are columbids, have a pointed, high aspect ratio wing, and use a 'tip-reversal'

upstroke during slow flight (Tobalske et al., 2003). We hypothesized that this variation in wing kinematics may be crucial, as the positioning of the wings during the first upstroke appears to play a prominent role in the initial phase of take-off. Tip-reversal upstroke may enhance aerodynamic force production at this important phase, even prior to the first downstroke. Indeed, it has been found that wings of birds using a tip-reversal upstroke (such as pigeons, rock dove *Columba livia*) are capable of producing substantial aerodynamic forces in the upstroke posture (Crandell and Tobalske, 2011). Moreover, pigeons can generate aerodynamic forces during tip-reversal upstroke in low speed turns (Ros et al., 2011).

We combined kinematic and dynamic analyses with particle image velocimetry (PIV), focusing on the first three wingbeats after lift-off. Previous analysis of starling and quail (Earls, 2000) measured take-off from a flat platform, which may heavily influence aerodynamic performance *via* complex interactions with the ground (Doligalski et al., 1994; Han and Cho, 2005). Thus, our recordings were performed for a take-off from a perch. Through our novel exploration of aerodynamic performance, we aimed to provide a more comprehensive understanding of the transition from terrestrial to aerial forces during take-off.

MATERIALS AND METHODS

Animals

Seven zebra finches [*T. guttata* Reichenbach 1862; mean body mass (m) ± s.d., 15.4±1.8 g] and three diamond doves [*G. cuneata* (Latham 1801); 51.0±5.1 g] were purchased from commercial dealers, housed in flight cages, and provided with food and water *ad libitum*. Kinematics and force data collection were performed at the Muséum National d'Histoire Naturelle (MNHN) in Paris for three of the seven zebra finches according to French legislation. Kinematics, force and PIV data collection were performed at the Field Research Station in Missoula, MT, USA, for four zebra finches and all three diamond doves. The animals were trained to take-off from a perch at a climb angle of ~45 deg. All care and experimental procedures were approved by the University of Montana IACUC. We obtained morphometrics of these animals using standard techniques with the wings spread as in mid-downstroke (Tobalske et al., 2004) (Table 1). Herein, we report single wing length (cm), body width between the wings (cm), single wing projected surface area (cm^2), mean wing chord (calculated as the width of the wing at one-third distance from the shoulder, cm), aspect ratio (wing span divided by mean wing chord, dimensionless) and tarsometatarsus length (cm).

Kinematics

At MNHN, four digital high-speed video cameras (AVT Pike F-032B, Alliance Vision Technologies, Stadtroda, Germany) were positioned around the perch and take-offs were recorded at 200 Hz with a shutter speed of 300 µs. The cameras were set in lateral, dorsal, oblique–frontal and frontal views and the overlapping fields of view of the cameras enabled a 3D reconstruction of the bird's movements during take-off, as well as during three complete wingbeat cycles after take-off. A checkerboard composed of 81 squares of 10×10 mm was used to calibrate the cameras and scale the images. A MatLab (R2011b, Mathworks Inc., Natick, MA, USA) custom-written M-file (Loco 3.3, Paul-Antoine Libourel MNHN) was used to extract the edge of the animal (head, tail and wings excluded) and calculate the coordinates of the centre of gravity from this shape (supplementary material Fig. S1). The tip of the 9th primary of the left wing was digitized for the same trials. The digitization provided four sets of 2D coordinates for the centre of gravity and for the tip of the wing, used to calculate the 3D coordinates with a direct linear transform (DLT) routine (Hartley and Sturm, 1997). At the Field Research Station in Missoula, methods were similar, but we used four synchronized cameras, recording at 500 Hz and with a shutter speed of 143 µs. These included two Photron 1024 PCI (Photron Inc., San Diego, CA, USA), one Photron SA-3 and one Phantom MiroEx4 (Vision Research Inc., Wayne, NJ, USA). The reconstruction of the centre of gravity of the shape formed by the edge of the bird was used as a proxy for the bird's centre of mass. A calculation of the actual centre of mass position using the multiple suspension method (Abourachid, 1993) for three zebra finches revealed that this centre of mass approximation was satisfactory: the distance between the centre of gravity of the edge of the shape and the actual centre of mass was 6.4±3.9 mm, less than 7% of total length of the bird and less than 15% of maximal body width of the bird (supplementary material Fig. S1). As birds flew within a vertical plane, approximately perpendicular to the perch, this point was used to calculate the 2D trajectory of the animal (supplementary material Fig. S2).

The trajectory of the animals was imposed by perch placement, which were set 0.75 m apart and inclined so that a line connecting the perches would be at 4 deg above horizontal. Otherwise, the chosen flight path was not constrained, and variability of both the trajectory and body angle was relatively small. The mean magnitude of absolute deviations from the trajectory was 6.7±3.2 cm and varied from 0 to 13.5±3.3 cm for zebra finch. In diamond dove, the mean magnitude of absolute deviations from the trajectory was 5.4±3.6 cm and varied from 0 to 10.9±3.8 cm. Body orientation was 16±5 deg from horizontal for zebra finch and 21±4 deg for diamond dove (supplementary material Fig. S2).

The component and resultant velocities ($m\,s^{-1}$) and accelerations ($m\,s^{-2}$) were calculated as the first and second derivatives of the trajectory, respectively. A MatLab (R2011b, The Mathworks Inc.) script allowed the reconstruction of the global orientation of the digitized shape, which was used to calculate the body angle (in deg), corresponding to the angle between the body and the horizontal (supplementary material Fig. S2).

The vertical trajectory of the tip of the 9th primary was used to define flight phases as it describes a succession of local maxima and minima that match upstroke/downstroke transition (USDS) and downstroke/upstroke transition (DSUS), respectively. The average of the wingbeat duration was calculated at different take-off phases. The beginning of the first upstroke was extracted (first use of the wings, FW) as well as lift-off (LO) corresponding to the last touch of the perch by the toes.

In our analysis, take-off was divided into four phases (Fig. 1E): (1) start of take-off (t_0), when the bird is motionless on the perch, with folded wings and initiates counter-movement, (2) wing and leg extension, when the bird is still on the perch, (3) first downstroke and loss of foot contact with perch (lift off, LO), (4) subsequent wingbeats with leg retraction against the body.

Table 1. Morphometric parameters of zebra finch (*Taeniopygia guttata*) and diamond dove (*Geopelia cuneata*)

Species	Wing length (cm)	Body width (cm)	Wing area (cm^2)	Wing chord (cm)	Aspect ratio	Tarsometatarsus length (cm)
Zebra finch	7.5±0.4	2.4±0.2	27.2±2.3	4.1±0.2	4.2±0.04	1.6±0.03
Diamond dove	12.0±0.4	2.8±0.2	56.8±4.8	5.5±0.1	4.9±0.05	1.7±0.1

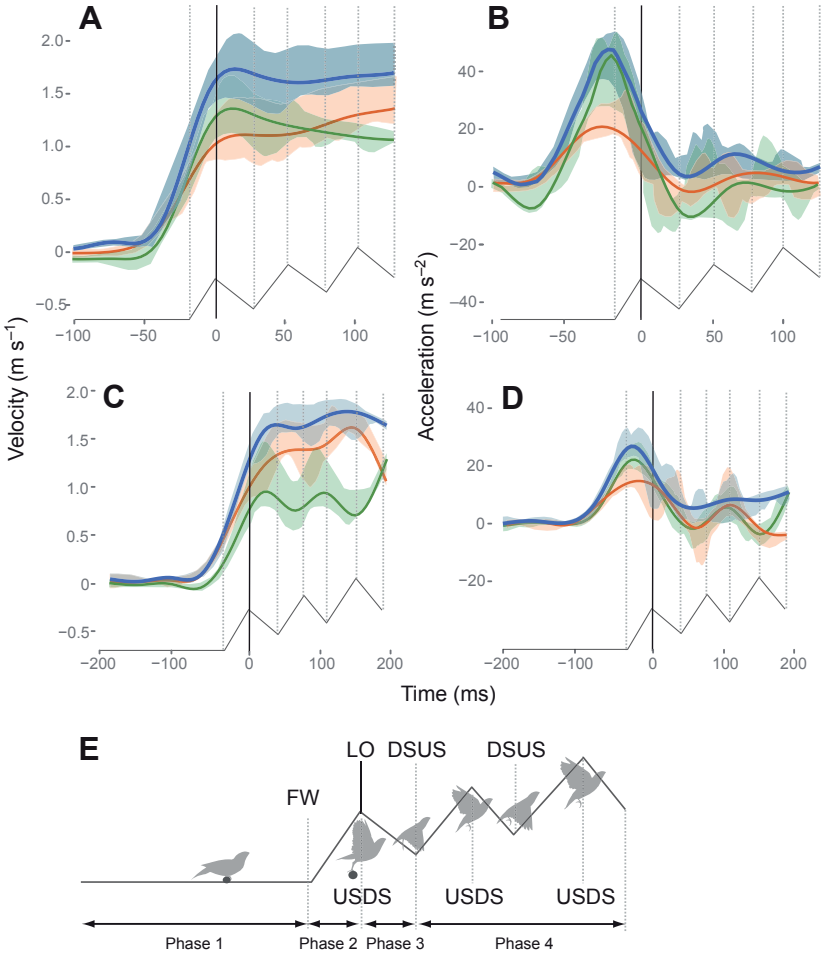

Fig. 1. (A,C) Velocity and (B,D) acceleration, calculated from the displacement of the geometric centre of the animal during take-off in zebra finch (*Taeniopygia guttata*, A,B) and diamond dove (*Geopelia cuneata*, C,D). *N*=7 zebra finches and *N*=3 diamond doves for 5 trials within each bird. Shading illustrates the variability, defined as the maximum–minimum range across all trials. Orange, the horizontal component; green, the vertical component; blue, the resultant (V_{RK} and $\dot{V}_{RK}$). (E) Sketch of the upstroke/downstroke succession during take-off. USDS, upstroke/downstroke transition; DSUS, downstroke/upstroke transition; LO, lift-off; FW, first use of the wings.

We calculated resultant acceleration using kinematic data ($\dot{V}_{RK}$):

$$\dot{V}_{RK} = \sqrt{\dot{V}_{XK}^2 + \dot{V}_{YK}^2 + \dot{V}_{ZK}^2}\ , \quad (1)$$

where $\dot{V}_{XK}$ is forward kinematic acceleration, $\dot{V}_{YK}$ is lateral kinematic acceleration and $\dot{V}_{ZK}$ is vertical kinematic acceleration. We calculated mean kinematic acceleration on the first upstroke duration (t_{up}, in ms). Mean $\dot{V}_{RK}$ was compared with resultant acceleration calculated from the average ground reaction force ($\dot{V}_{RFP}$, see below) during this period. Resultant acceleration calculated from the kinematics was also averaged on the duration of each wingbeat (t_{wb}, in ms) from the start of upstroke to the start of the next upstroke). This mean $\dot{V}_{RK}$ was compared with resultant acceleration calculated using PIV data ($\dot{V}_{RPIV}$, see below).

Ground reaction forces

At MNHN, a wooden perch 1.5 cm in diameter and 8.5 cm long was mounted on a force platform (Squirrel force plate, Kistler France, Les Ulis, France; resolution ±0.01 N) with a top plate of 20×10 cm, attached to a charge amplifier (type 9865, Kistler France). It was used to record the vertical and horizontal ground reaction forces exerted on the perch at 400 Hz, using BioWare Software Version 4.0.x Type 2812A (Kistler France).

At the Field Research Station in Missoula, the force perch was 1.3 cm in diameter, 7 cm in length. It was covered in sandpaper to provide traction. The perch was mounted with its axis in line with the surface of a custom-made Bertec force plate (15×15 cm platform, 200 Hz resonant frequency, Bertec Corp., Columbus, OH, USA). Forces on the Bertec plate were digitally amplified 10× (Bertec AM6800) and recorded at 500 Hz using Chart software v4.5 (ADInstruments, Inc., Colorado Springs, CO, USA) and a Powerlab 8 SP A/D converter (ADInstruments Inc.).

Forces were filtered using a zero phase shift low-pass (50 Hz) Butterworth filter. The resultant acceleration, measured using the force plate ($\dot{V}_{RFP}$) was calculated:

$$\dot{V}_{RFP} = \frac{\sqrt{\mathbf{F}_X^2 + \mathbf{F}_Y^2 + (\mathbf{F}_Z - m\boldsymbol{g})^2}}{m}\ , \quad (2)$$

where $\mathbf{F}_X$ is forward force, $\mathbf{F}_Y$ is lateral force and $\mathbf{F}_Z$ is vertical force. For comparison with mean $\dot{V}_{RK}$ during the first upstroke (i.e. during ground contact), we averaged $\dot{V}_{RFP}$ on t_{up}.

To measure the relative hindlimb contribution to initial resultant flight velocity (i.e. percentage of $\dot{V}_{RK}$ encompassed by $\dot{V}_{RFP}$) at LO, we followed the methods of Earls (Earls, 2000) and integrated $\dot{V}_{RFP}$ with respect to time (t) from the beginning of take-off (t_0) to LO:

$$V_{RFP} = \int_{t_0}^{LO} \frac{\sqrt{\mathbf{F}_X^2 + \mathbf{F}_Y^2 + (\mathbf{F}_Z - m\boldsymbol{g})^2}}{m} dt\ . \quad (3)$$

PIV

To compare aerodynamics with associated wingbeat kinematics, we used a synchronized high-speed video camera (Photron 1024 PCI, Photron Inc.) sampling at 500 Hz, and located lateral to the animal. Data acquisition and analysis of PIV were performed using a

LaVison GmBH (Goettingen, Germany) PIV system running DaVis 7.1 software. A dual-cavity pulsed 50 mJ Nd:YAG laser was used to illuminate a 3 mm thick flow field, with planar dimensions spanning a field of 25×33 cm. The illumination field was cranial to the bird, parasagittal and mid-wing at the middle of downstroke (Spedding et al., 2003; Warrick et al., 2005). We seeded the air with particles of olive oil (<1 μm in diameter) generated at a rate of 7×10^{10} particles s^{-1} using a vaporizer fitted with a Laskin nozzle. Particle illumination was recorded using a 1376×1040 pixel, charged-coupled device (CCD) camera placed perpendicular to the illumination field, and PIV samples were obtained at 5 Hz. To calculate particle velocity, we used cross-correlation of paired images with an elapsed time between images (Δt) of 500 μs. Mean particle separation was 6 pixels in the centre of the animal's wake. We employed an adaptive multipass filter with an initial interrogation area of 64×64 pixels and a final area of 16×16 pixels with 50% overlap. Vector fields were post-processed using a median filter [strong removal if difference relative to mean >3× root mean square (r.m.s.) of neighbours and iterative reinsertion if <3× r.m.s. of neighbours], removal of groups with <5 vectors, filling of all empty spaces by interpolation, and one pass of 3×3 smoothing. Subsequent analysis focused upon vortex cores.

We used streamlines, drawn with vectors expressed relative to mean velocity, to inform our selection of regions of vorticity (ω, s^{-1}), which is a measure of local change in velocity in the flow field (Spedding et al., 2003). We treated as background noise and masked from subsequent analysis $|\omega|<3$ s.d. of $|\omega|$ in the free-stream. To measure circulation (Γ, $m^2 s^{-1}$) in vortex cores, we used an adaptation of previously published methods (Spedding et al., 2003). We integrated all same-sign ω in a given PIV field within 1.5 chord lengths of peak ω to measure Γ. We considered each negatively signed vortex core deposited in the wake during early downstroke to represent the cross-section of a starting vortex shed from the trailing edge of the wing, equal in magnitude but opposite in sign from the bound vortex on the wing as lift development began during downstroke. Similarly, we considered each positively signed vortex core deposited in the wake during late downstroke to represent the cross-section of an ending vortex shed from the trailing edge of the wing.

We estimated mean lift during the entire wingbeat (L) by coupling our PIV data with separately acquired 3D kinematic data for the same test subjects (Spedding et al., 2003; Warrick et al., 2005; Tobalske and Dial, 2007) (see 'Kinematics', above). Note that L includes vertical (weight support) and horizontal (thrust) components. L was estimated according to Eqn 4:

$$L = \rho \frac{A(\Gamma + cSV_{\text{vort}})}{t_{\text{wb}}} , \quad (4)$$

where ρ is air density (air density in Missoula at 1000 m in altitude is 1.06±0.01 kg m^{-3}), A is the area swept by the two wings during each downstroke, not including the body, c is added-mass coefficient (Dabiri, 2005), S is mean diameter of observed vortex cores and V_{vort} is self-induced vortex velocity (Dabiri, 2005). As elsewhere (Spedding et al., 2003; Warrick et al., 2005), we assumed that a single vortex loop was shed per downstroke and that no contraction occurred during wake development. We assumed c=0.72 as the added-mass coefficient previously reported for an elliptical vortex (Dabiri, 2005). We measured V_{vort} as observed rate of translation of ω_{max} in the subset (N=37 for zebra finch and N=42 for diamond dove) of our PIV samples in which the same vortex core appeared in consecutive images. We also measured the magnitude and angle from horizontal for induced velocity (m s^{-1}) in the middle of the shed vortices (Tobalske and Dial, 2007).

We estimated mean acceleration using the PIV data ($\dot{V}_{\text{RPIV}}$), which was the acceleration due to aerodynamic force produced during each wingbeat with gravity subtracted:

$$\dot{V}_{\text{RPIV}} = \frac{L}{m} - \boldsymbol{g}. \quad (5)$$

Therefore, when $\dot{V}_{\text{RPIV}}$ is negative, the acceleration produced by the wings does not support body weight.

Advance ratio

To provide insight into the potential for wing–wake interaction and other unsteady aerodynamic effects (Spedding, 1993; Dickinson et al., 1999) to dominate wing function during take-off, we calculated advance ratio (dimensionless) using kinematic data (J_{K}) and using kinematics coupled with PIV data (J_{PIV}). Advance ratio in aeronautical engineering is an expression of aircraft velocity divided by the tip velocity of the aircraft's propeller, or, equivalently, distance travelled by the aircraft relative to the excursion of the propeller tip during one revolution (Vogel, 1994). Rather than assume sinusoidal motion of the oscillating wing as is traditionally done when adapting propeller equations to model advance ratio in animals that oscillate their wings (Ellington, 1984; Vogel, 1994), we used observed 3D wingtip velocity relative to the bird (V_{wtip}). Thus:

$$J_{\text{K}} = \frac{V_{\text{RK}}}{V_{\text{wtip}}} \quad (6)$$

and

$$J_{\text{PIV}} = \frac{D_{\text{wake}}}{t_{\text{wb}} V_{\text{wtip}}} , \quad (7)$$

where D_{wake} is the mean distance (in meters) between vortices in the wake. Note that Eqn 7 includes the contribution of self-convection of shed vortices:

$$\frac{D_{\text{wake}}}{t_{\text{wb}}} \cong V_{\text{RK}} + V_{\text{vort}} . \quad (8)$$

J_{PIV} was undefined for wingbeat 1, as it lacks a previously shed vortex (D_{wake} was undefined).

Statistics

To test for differences in the timing of first downstroke and LO, we used two-way repeated measures ANOVA with time and individual as factors and taking into account the trial repetition and species.

We also used two-way repeated measures ANOVA to test for a statistically significant difference between wingbeat 1 and subsequent wingbeats for L, the angle magnitude of induced velocity in the wake and J_{K}. Wingbeat and individual were used as factors and the trial repetition was also taken into account for both species.

Lastly, t-tests were used to compare data sets obtained from kinematic analysis with data sets obtained from ground reaction force or aerodynamic analyses. All statistical tests were performed using R package (*stats* version 2.15.0) (R Development Core Team, 2010). Throughout, we report means ± s.d.

RESULTS

Kinematics

During the preparation to take-off, each bird crouched from a standing position. This counter-movement (starting at time t_0) was visible in both species but was more evident in diamond dove, with

a lower body angle before LO (16.3±5.3 deg) compared with the zebra finch (20.1±7.3 deg) (supplementary material Fig. S2). During the second phase of take-off, the birds started extending their hindlimbs and forelimbs. This happened 28.3±7.6 ms before LO in zebra finch compared with 38.9±8.10 ms before LO in diamond dove. This is about 80% and 60% of the time from the start of counter-movement (t_0) to LO in the zebra finch and diamond dove, respectively. Both species started their first downstroke after their feet were completely off the perch (2 ms delay in the zebra finch, 6 ms in the diamond dove). However, these differences in timing were not statistically significant (zebra finch: ANOVA, factor=timing, $F_{1,26}$=0.01, P>0.9; factor=individual, $F_{1,3}$=0.02, P>0.7; diamond dove: ANOVA, factor=timing, $F_{1,9}$=4.9, P>0.06; factor=individual, $F_{1,2}$=0.04, P>0.2) and it should be noted that 2 ms was the margin of error for our video sampling at 500 Hz. The first wingbeat ended 24.5±6.1 ms after lift-off in zebra finch compared with 37.9±6.2 ms in diamond dove. In zebra finch, each wingbeat lasted approximately 50 ms, compared with 70 ms in diamond dove. These durations are nearly equivalent in terms of the total wingbeat cycle, at 52.3% in the zebra finch and 54.1% in the diamond dove.

In both species, V_{RK} (velocity calculated using kinematic data) increased during the first two phases of take-off (Fig. 1A,C). In zebra finch, V_{RK} increased from 0.03±0.03 m s^{-1} at t_0 to 1.74±0.3 m s^{-1} at LO. In diamond dove, V_{RK} increased from 0.04±0.1 m s^{-1} at t_0 to 1.29±0.1 m s^{-1} at LO. After LO, V_{RK} remained fairly constant during the first three wingbeats and reached 1.8±0.6 m s^{-1} in zebra finch and 1.7±0.1 m s^{-1} in diamond dove. V_{RK} at LO corresponded to 92.3±4.2% of the maximal V_{RK} reached during the first wingbeat in zebra finch and 79.4±3.9% in diamond dove.

The acceleration profile shows a peak during the perching phase of take-off. In zebra finch, $\dot{V}_{RK}$ reached 47.2±14.4 m s^{-2} (4.8 × body weight), and occurred 28.3±6.0 ms before LO (Fig. 1B). In diamond dove, $\dot{V}_{RK}$ reached 26.7±3.2 m s^{-2} (2.7 × body weight) and occurred 23.5±7.9 ms before LO (Fig. 1D). These times are 80.6% and 76.5% of the interval between t_0 and LO in zebra finch and diamond dove, respectively.

Force production of the legs

The $\dot{V}_{RPF}$ produced during take-off, calculated using the ground reaction force, reached 47.8±7.5 m s^{-2} in zebra finch compared with 26.7±7.0 m s^{-2} in diamond dove (Fig. 2A,C). Thus, the maximal leg force produced by the animal corresponds to (4.9±0.7) × body weight for zebra finch and (2.7±0.3) × body weight for diamond dove. Mean $\dot{V}_{RPF}$ during the first upstroke was 35.5±18.0 m s^{-2} in zebra finch and 25.2±8.8 m s^{-2} in diamond dove (Fig. 4). The peak V_{RPF} was 1.78±0.6 m s^{-1} at LO in zebra finch and 1.2±0.4 m s^{-1} in diamond dove (Fig. 2B,D).

Force production of the wings

For zebra finch, the first wingbeat produced significantly less L than the second and third ones (Fig. 3) (ANOVA, factor=wingbeat, $F_{1,27}$=16.03, P<0.001; factor=individual, $F_{1,3}$=0.9, P>0.1). Therefore, for the first wingbeat, L represented (0.9±0.4) × body weight, whereas it comprised (1.4±0.6) × body weight for the second wingbeat and (1.7±0.2) × body weight for the third. The $\dot{V}_{RPIV}$ produced during the first wingbeat was 58±3.4% of that during the second and third wingbeats (Fig. 4A). Considering the relevant variables for estimating L (Eqn 4; Table 2) the differences were due to less circulation (Γ), a smaller area (A) of the vortex loop and a lower induced velocity during the first wingbeat, compared with the subsequent wingbeats. The angle of the induced velocity in the wake for all three wingbeats was not significantly different among wingbeats (ANOVA, factor=wingbeat, $F_{1,18}$=0.11, P>0.7; factor=individual, $F_{3,18}$=2.3, P<0.1). Although the general trend was for induced velocity to increase with wingbeat number, high variability meant that induced velocity of the first wingbeat, 3.9±1.8 m s^{-1}, was not significantly less than those of the second (5.1±2.3 m s^{-1}) and third wingbeat (5.1±1.6 m s^{-1}).

For diamond dove, the first wingbeat also produced significantly less L than the subsequent ones (ANOVA, factor=wingbeat, $F_{1,35}$=5.6, P<0.05; factor=individual, $F_{1,2}$=1.6, P>0.2). For the first wingbeat, L was (0.9±0.3) × body weight, and it was (1.1±0.0.3) × body weight for the second wingbeat and (1.7±0.6) × body weight

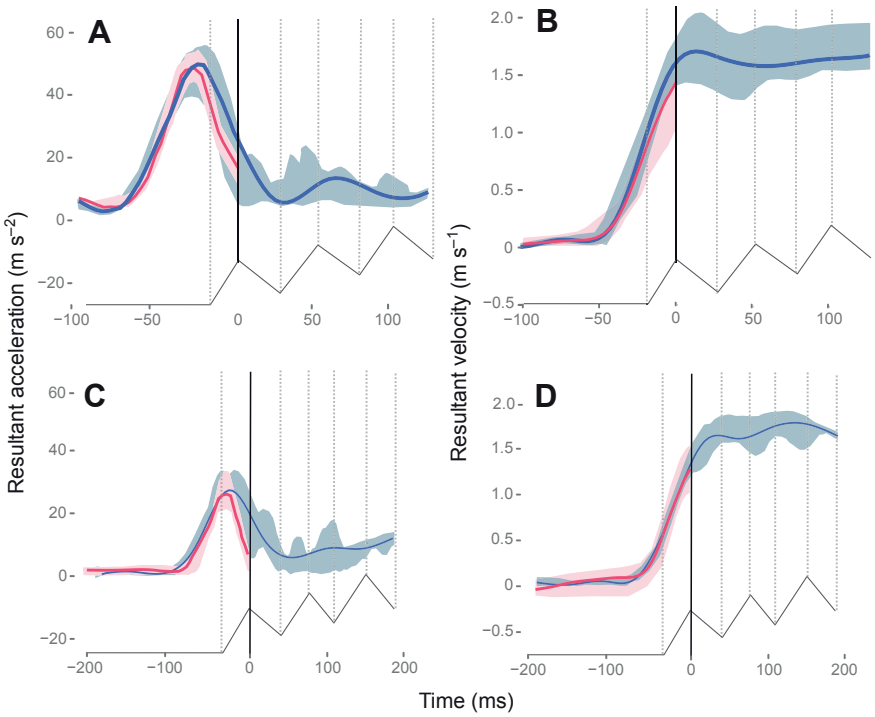

Fig. 2. Resultant acceleration ($\dot{V}_{RK}$, A,C) and resultant velocity (V_{RK}, B,D), calculated from the kinematic data (in blue) and from the force measurements ($\dot{V}_{RFP}$ and V_{RFP} in pink) in zebra finch (*T. guttata*, A,B) and diamond dove (*G. cuneata*, C,D).

Table 2. Aerodynamic parameters for the first three wingbeats after LO in zebra finch and diamond dove

	Wingbeat 1	Wingbeat 2	Wingbeat 3
Zebra finch (*Taeniopygia guttata*)			
A (cm^2)	163.64±17.7	193.82±22.3	177.88±6.5
Γ ($m^2 s^{-1}$) (+)	0.35±0.1	0.42±0.2	0.5±0.02
Γ ($m^2 s^{-1}$) (–)	–0.36±0.1	–0.54±0.1	–0.47±0.1
S (mm)	0.01±0.001	0.01±0.001	0.01±0.001
V_{vort} ($m.s^{-1}$)	0.59±0.13	0.68±0.2	0.79±0.05
t_0 (ms)	44.94±5.7	39.73±4.4	39.0±3.8
Angle of induced velocity to horizontal (deg)	63.57±6.7	60.19±11.8	54.6±4.9
Magnitude of induced velocity ($m s^{-1}$)	3.9±1.9	5.1±2.3	5.1±1.6
V_{wtip} ($m s^{-1}$)	6.0±1.5	9.3±0.4	9.8±0.5
D_{wake} (m)	–	0.15±0.01	0.16 + 0.01
J_K	0.32±0.10	0.20±0.02	0.20±0.03
J_{PIV}	–	0.37±0.04	0.44±0.03
Diamond dove (*Geopelia cuneata*)			
A (cm^2)	461.34±40.9	462.66±33.4	399.2±40.4
Γ ($m^2 s^{-1}$) (+)	0.58±0.2	0.71±0.1	0.46±0.1
Γ ($m^2 s^{-1}$) (–)	–0.76±0.3	–0.79±0.1	0.57±0.1
S (mm)	0.01±0.001	0.01±0.001	0.01±0.001
V_{vort} ($m s^{-1}$)	0.87±0.14	1.22±0.05	1.22±0.05
t_0 (ms)	64.0±6.4	65.18±5.2	67.3±2.3
Angle of induced velocity to horizontal (deg)	54.92±10.1	69.59±6.1	70.6±10.1
Magnitude of induced velocity ($m s^{-1}$)	4.37±1.3	5.22±1.3	4.0±0.8
V_{wtip} ($m s^{-1}$)	9.1±1.7	11.4±0.6	9.6±0.4
D_{wake} (m)	–	0.25±0	0.20±0.01
J_K	0.20±0.05	0.17±0.01	0.19±0.02
J_{PIV}	–	0.24±0.01	0.30±0.02

Data are means ± s.d.
Diamond dove data for wingbeat 3 come from another experiment with the same methods but where birds were using level flight instead of climbing flight.

for the third wingbeat. The first wingbeat comprised 63±5.2% of $\dot{V}_{RPIV}$ produced during the subsequent wingbeats (Fig. 4B). As in the finch, less L was associated with less Γ and a lower induced velocity in wingbeat 1 (Table 2). The angle of the induced velocity for the first wingbeat was significantly lower than that for the second (ANOVA, factor=wingbeat, $F_{1,23}$=43.5, P<0.001; factor=individual, $F_{2,23}$=1.8, P>0.1). Induced velocity for the first wingbeat was 4.4±1.3 $m s^{-1}$, and it was 5.2±1.1 $m s^{-1}$ for the second wingbeat. These values were statistically different (ANOVA, factor=wingbeat, $F_{1,32}$=8.7, P<0.006; factor=individual, $F_{2,32}$=2.8, P>0.07).

Comparison of wing and leg contributions

During the first phase of take-off, when the bird was on the perch with folded wings, V_{RPF} was similar to V_K in both species (for zebra finch: t-test, d.f.=13, P>0.7; for diamond dove: t-test, d.f.=12, P>0.5) (Fig. 2B,D). $\dot{V}_{RPF}$ and $\dot{V}_{RK}$ followed a similar pattern in both species (for zebra finch: t-test, d.f.=13, P>0.6; for diamond dove: t-test, d.f.=12, P>0.21) (Fig. 2A,C). This means that during the first phase of take-off the legs are responsible for the entire resultant velocity and resultant acceleration.

During the second phase of take-off, when the wings were unfolded, $\dot{V}_{RPF}$ was not significantly different from $\dot{V}_{RK}$: 34.56±7.9 $m s^{-2}$ for $\dot{V}_{RPF}$ compared with 33.8±6.45 $m s^{-2}$ for $\dot{V}_{RK}$ in zebra finch, and 24.51±3.18 $m s^{-2}$ for $\dot{V}_{RPF}$ compared with 23.4±1.8 $m s^{-2}$ for $\dot{V}_{RK}$ in diamond dove (Fig. 4) (for zebra finch: t-test, d.f.=13, P>0.05; for diamond dove: t-test, d.f.=12, P>0.05). Moreover, at LO, $\dot{V}_{RPF}$ was 93.6±0.6% of the $\dot{V}_{RK}$ in zebra finch, and 95.2±0.4% of $\dot{V}_{RK}$ in diamond dove (Fig. 2B,D).

After LO, the $\dot{V}_{RK}$ during the first wingbeat was significantly different from $\dot{V}_{RPIV}$ (for zebra finch: t-test, d.f.=13, P<0.001; for diamond dove: t-test, d.f.=12, P<0.001). But note, for wingbeat 1, $\dot{V}_{RK}$ was approximately equal to the sum of $\dot{V}_{RFP}$ and $\dot{V}_{RPIV}$.

During the following wingbeats (Fig. 4), there was no significant difference between $\dot{V}_{RPIV}$ and $\dot{V}_{RK}$ (for the second wingbeat in zebra finch: t-test, d.f.=13, P=0.37; for diamond dove: t-test, d.f.=12, P=0.20).

Advance ratio measured using kinematics (J_K) did not differ significantly between wingbeats (for zebra finch: ANOVA, factor=wingbeat, $F_{2,3}$=3.0, P>0.1; factor=individual: $F_{1,3}$=0.14, P>0.7; for diamond dove: ANOVA, factor=wingbeat, $F_{2,3}$=0.65, P>0.5; factor=individual, $F_{1,3}$=0.03, P>0.8), or among species (ANOVA, factor=species, $F_{1,14}$=3.31, P>0.09; factor=individual, $F_{1,14}$=0.14, P>0.7).

However, J_{PIV} was significantly larger in zebra finch (~0.40) compared with diamond dove (~0.30) during wingbeats 2 and 3 (t-test, d.f.=5, P<0.0003), and J_{PIV} was always greater than J_K (t-test, d.f.=11, P<0.0001), which varied from 0.17 to 0.32 (Table 2).

DISCUSSION

The wings of birds have historically been considered as the primary force producers during take-off (Rüppell, 1975; Heppner and Anderson, 1985). However, more recent studies (Earls, 2000; Tobalske et al., 2004; Berg and Biewener, 2010) indicate that the legs play a key role in producing the acceleration needed for take-off. By combining three different data sets to calculate force production, we were able to assess the relative role of both hindlimbs and forelimbs through take-off in two other species of birds with different wing shape and ecology. Our data show that in zebra finch, a small passerine, and in diamond dove, a small columbid, the hindlimbs and forelimbs are used successively, with hindlimb dominance in the first phases of take-off providing initial acceleration, and coordinated use of wings to maintain velocity through the first three wingbeats. Despite dramatic differences in body size, wing morphology (Table 1) and slow-flight kinematics

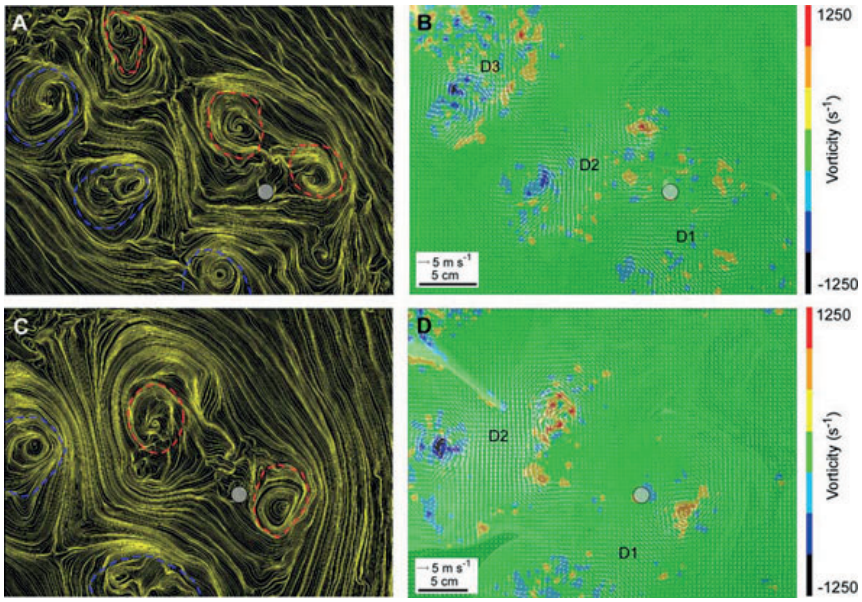

Fig. 3. Particle image velocimetry (PIV). (A,C) Velocity vectors, expressed relative to mean velocity, and with background vorticity (ω). (B,D) Streamlines associated with the vector field. Broken lines indicate regions sampled for ω (red, starting vortex; blue, ending vortex) in zebra finch (*T. guttata*, A,B) and diamond dove (*G. cuneata*, C,D). Grey circle highlights the location of the take-off perch. D1–3 corresponds to downstroke 1 to 3.

(Tobalske, 2007), we did not observe significant differences between species in aerodynamic force produced. Rather, the most prominent difference between birds was observed at the initial acceleration – due almost exclusively to the hindlimbs – and subsequent flight velocity upon leaving the perch, both of which were greater in the zebra finch than in the dove.

During the first phase of take-off, the resultant acceleration calculated from the force data ($\dot{V}_{RFP}$) was not significantly different from the resultant acceleration calculated from the kinematics data ($\dot{V}_{RK}$, Figs 1, 2), indicating that the legs were wholly responsible for the acceleration while in contact with the perch during the preparation for take-off. An acceleration peak was observed in both species, with a magnitude four times greater than that observed after LO. This acceleration peak occurred at the transition between the first and the second phase of take-off in zebra finch (28.3±6.0 ms before lift-off) whereas it happened slightly after the beginning of the first upstroke in diamond dove (15.35±4.2 ms after the beginning of the second phase) (Fig. 1B,D). For both birds, this acceleration peak occurred while the bird was still on the perch. The observed maximal vertical force production ($\mathbf{F}_z$) was greater than that reported in other studies: 1.3–2.3 × body weight in pigeon compared with 2.9–3.6 × body weight in diamond dove and 3.6–8.3 × body weight in zebra finch (Clark and Alexander, 1975; Heppner and Anderson, 1985; Bonser and Rayner, 1996). We also observed that relative hindlimb forces produced by the dove (m=50 g) were 55±2.5% lower than in the finch (m=15 g), which was consistent with the hypothesis that the maximal acceleration generated across species should be inversely proportional to body weight (Bonser and Rayner, 1996).

In the second phase of take-off, corresponding to the first upstroke, the mean $\dot{V}_{RFP}$ represented 93±0.6% of the resultant acceleration calculated from the kinematics data for zebra finch and 92.1±0.4% for diamond dove (Fig. 4). This indicates a combined action of the hindlimbs with the forelimbs, although the hindlimbs dominated. The wings started to unfold at the same moment as the acceleration profiles of ground reaction forces and kinematics start to diverge (Fig. 2A,C). We suggest that forces produced by the wings (Crandell and Tobalske, 2011; Ros et al., 2011) may be responsible for a part of the observed disparity between ground reaction forces and observed kinematics in diamond dove. However, it seems unlikely that zebra finch is generating an aerodynamically active upstroke, as the species uses a flexed-wing upstroke (Tobalske et al., 1999), and no aerodynamic activity was visible in the wake. The bird's body is rotating upward as its legs are extending and this rotational kinematics acceleration might be added inappropriately to our linear $\dot{V}_{RK}$, thus leading to an overestimation of its magnitude. In any case, our data show that in both species, the initial acceleration peak is predominantly due to the hindlimbs, with the legs contributing to approximately 70–80% of $\dot{V}_{RK}$ produced during the second phase of take-off.

Surprisingly, despite large differences in leg and wing morphology (Table 1), the two species appear to promote similar tactics of wing and leg use. However, in comparing maximal velocity of the first wingbeat (V_{RK}) with that produced by the legs (V_{RFP}) at LO, an interesting pattern emerges. In zebra finch, 92.3±4.2% of the maximal velocity was reached by LO, whereas only 79.36±3.9% was reached in diamond dove (Fig. 2B,D). Observed velocities produced by the leg forces were at the high end of the range that has previously been reported for European starling, Japanese quail, rufous hummingbird and pigeon, for which the percentage of velocity reached at LO corresponds to between 59% and 90% of the velocity achieved at the next USDS (Earls, 2000; Tobalske, 2004; Berg and Biewener, 2010). In comparing the magnitude of resultant acceleration previously reported with data from the present study, we see that both the zebra finch (4.4 m s^{-2}) and diamond dove (3.4 m s^{-2}) had values near those of the European starling (4.3 m s^{-2}) (Earls, 2000). All three of these species are ecological generalists in their respective habitats, and the legs contribute to 92%, 79% and 95% of total velocity, respectively, by take-off. In contrast, the resultant acceleration of a highly specialized aerial bird, the rufous hummingbird, is 1.78 m s^{-2} with the legs contributing to only 60% of total velocity (Tobalske et al., 2004). At the other end of the spectrum, the Japanese quail, a ground specialist, produces an acceleration maximum of 8.3 m s^{-2}, contributing to 89% body velocity. This continuum suggests the interaction between wings and legs should be placed in an ecological context, and merits further exploration with a larger sample size.

In both zebra finch and diamond dove, the beginning of the first downstroke occurs a few milliseconds after the bird leaves the perch, resulting in a discrete succession in the use of the hindlimbs and forelimbs. However, we note that the relative timing of the different

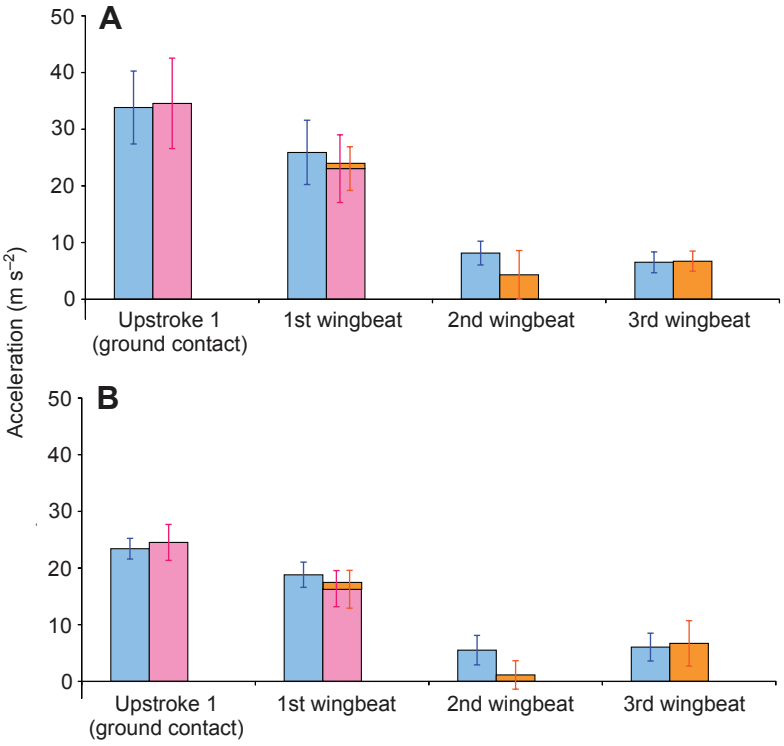

Fig. 4. Category plot of the acceleration produced during the first upstroke and the first three wingbeats in zebra finch (*T. guttata*, A) and in diamond dove (*G. cuneata*, B). Blue, resultant acceleration calculated from kinematic data ($\dot{V}_{RK}$) for 5 trials in *N*=7 zebra finches and *N*=3 diamond doves during the first upstroke and during each wingbeat. Pink, resultant acceleration calculated from the force data ($\dot{V}_{RFP}$) for 5 trials in *N*=7 zebra finches and *N*=3 diamond doves during the first upstroke and first wingbeat. Orange, resultant acceleration calculated from PIV data ($\dot{V}_{PIV}$) with *N*=4 zebra finches and 37 wingbeats and *N*=3 diamond doves and 42 wingbeats.

phases of take-off is closely related to the animal's state of stress. Informally, we observed that the more stressed the bird was, the earlier the wings would start to be used, which is consistent with the previous studies on take-off (Earls, 2000; Tobalske et al., 2004). In this study, only trials with spontaneous, unstressed take-off were analysed, resulting in a low variability in the timing of take-off phases.

In the aerial phase of take-off, our data show that during the first wingbeat, the acceleration calculated from the PIV data ($\dot{V}_{RPIV}$) represented only 24.8±4.2% of $\dot{V}_{RK}$ in zebra finch and 29.9±3.6% in diamond dove. This further demonstrates that during the first wingbeat, the resultant acceleration is mostly due to the hindlimbs, with the wings contributing to about 30% of this acceleration. Moreover, we note that lift production (L) during the first wingbeat represents only 58±3.4% of the force produced by the subsequent wingbeats in zebra finch and 63±5.2% in diamond dove. Neither finches nor doves produced enough force in the first wingbeat to support body weight in the air – (0.9±0.4) and (0.9±0.3) × body weight, respectively – but, given the large standard deviations (Fig. 4), they may have supported body weight some of the time. Regardless, this minimal force production was not enough to accelerate quickly without relying on the initial acceleration of the legs. This was compensated for by the following wingbeats, where force production increased well above that required to support body weight (1.4 and 1.7 × body weight for finch and 1.1 and 1.7 × body weight for dove), indicating that force was used for net acceleration. Relatively large standard deviations for L and $\dot{V}_{RPIV}$ may also be linked to motivational differences between trials.

Both bird species followed a general pattern in force production by the wings, producing force near the minimal required to counter gravity and then increasing with subsequent wingbeats. This implies that generalist birds may have tuned the timing and magnitude of force production by the wings to accommodate neuromuscular, aerodynamic or environmental constraints. Our estimates of lift that increase with each wingbeat during take-off are consistent with direct measures of muscle activity in pigeons in which the pectoralis muscles are recruited at lower levels and produce lower force during the first wingbeat compared with subsequent wingbeats (Dial and Biewener, 1993; Tobalske and Biewener, 2008). Several mechanisms may explain this variation in force production. One hypothesis we suggest is that the birds may capitalize on a mechanism similar to wake recapture (Sane, 2003) in which the subsequent wingbeats are capable of capitalizing on induced flow from previous wingbeats. If this is the case, the first wingbeat is incapable of benefiting from induced flow, and may, therefore, exhibit weaker lift. Our observed low advance ratios (J_K and J_{PIV}; Table 2) suggest that wings may interact with previously shed circulation in the wake (Spedding, 1993). Even accounting for the contribution of self-convection of shed vortices away from the flying animal (V_{vort}), advance ratios were considerably less than 1 (J_{PIV}, Table 2). This revealed that the wingtips were always moving much further than the body during a given wingbeat. Another possible influence is the orientation of the body relative to the wake changes from first to subsequent wingbeats (Table 2; supplementary material Fig. S2), and body angle may initially be in an unfavourable orientation. In this case, the angle of induced downwash in the finch was not statistically different from that of the first and subsequent wingbeats, but for the diamond dove the angle of induced velocity was different, suggesting doves may be under pressure to reorient their body, but not finches. Finally, there may be a need to provide enough space for the wings to complete a full downstroke without hitting the substratum and risking wing damage (Heppner and Anderson, 1985). Thus, the wings are spatially limited and complete a smaller arc. Clearly, further studies of potential unsteady aerodynamic performance and the interactions between substrate and air are necessary.

In the zebra finch, the acceleration produced by the wings during the first wingbeat ($\dot{V}_{RK}$ and $\dot{V}_{RPIV}$) represents a lower proportion of the acceleration produced during the subsequent wingbeats than in diamond dove (Figs 2, 4). Diamond doves use a tip-reversal upstroke,

and we hypothesize that this style of upstroke is aerodynamically active (Crandell and Tobalske, 2011; Ros et al., 2011). Tip-reversal may provide an earlier onset of useful aerodynamic force production during the first wingbeat in diamond dove. Because of the interaction of body mass with acceleration in the present study, this suggestion must be interpreted as tentative. It would be useful to test this hypothesis within a clade that exhibits variation in body mass and upstroke style.

During take-off, the amount of acceleration produced by the hindlimbs is much higher than the acceleration produced by the forelimbs. This can be linked to the fact that it is more efficient to push against the ground than against the air (Dickinson et al., 2000). These data emphasize the prominent role of the hindlimbs in all avian locomotor behaviours except flight (Dial, 2003; Abourachid et al., 2011; Provini et al., 2012). This work suggests that during the transitional first wingbeat, a timing coordination exists between wings and legs, which can be seen as anatomical and neuromuscular systems, previously identified as 'modules' in birds (Gatesy and Dial, 1996). Our results combined with previous work (Earls, 2000; Tobalske et al., 2004) support the general conclusion underscoring the prominent role of hindlimbs during take-off in a phylogenetically, morphologically and ecologically diverse array of birds. More extensive phylogenetic analysis is warranted to test the generality of the hypothesis of a universal hindlimb drive during take-off in birds. But, if this pattern is universal, this would provide support for the leaping model for the origin of flight (Garner et al., 1999). Indeed, in cursorial theropod dinosaurs, powerful hindlimbs would have been a useful exaptation to a hindlimb-driven take-off. Moreover, in our study, we saw incremental use of the flight apparatus for the first wingbeat, as suggested by the work on WAIR (wing-assisted incline running) (Jackson and Dial, 2011) where birds use rapid flapping of the wings to run up inclined surfaces. Even though we studied a standing take-off instead of WAIR, our data suggest that incremental use of the pectoralis muscle can modulate leg performance and contribute to weight support, and thus this is a relevant model for the evolutionary origin of flapping. Therefore, our results may provide novel insights into the origin of avian flight as they are consistent with both leaping and WAIR models (Garner et al., 1999; Dial, 2003) with a hindlimb-driven take-off assisted by a gradual use of the forelimb through the first wingbeats.

LIST OF SYMBOLS AND ABBREVIATIONS

A	loop area of wake vortex
c	vortex added mass coefficient
DSUS	downstroke/upstroke transition
D_{wake}	distance between shed vortices
FW	first use of the wings
$\mathbf{F}_X$	forward force
$\mathbf{F}_Y$	lateral force
$\mathbf{F}_Z$	vertical force
$\boldsymbol{g}$	gravitational acceleration
J_K	advance ratio from kinematics
J_{PIV}	advance ratio from kinematics and aerodynamics
L	mean lift
LO	lift-off
m	body mass
PIV	particle image velocimetry
S	mean width of wake vortex
t	time
t_0	start of take-off with counter-movement
t_{up}	first upstroke duration
t_{wb}	full wingbeat duration
USDS	upstroke/downstroke transition
V_{RFP}	velocity calculated using data from force plate
$\dot{V}_{RFP}$	acceleration calculated using data from force plate
V_{RK}	velocity calculated using kinematic data
$\dot{V}_{RK}$	acceleration calculated using kinematics
$\dot{V}_{RPIV}$	average acceleration calculated from PIV and kinematics
V_{vort}	self-convection velocity of shed vortices
V_{wtip}	wingtip velocity
$\dot{V}_{XK}$	forward acceleration calculated from kinematics
$\dot{V}_{YK}$	lateral acceleration calculated from kinematics
$\dot{V}_{ZK}$	vertical acceleration calculated from kinematics
Δt	elapsed time between PIV paired images
Γ	circulation
ρ	air density
ω	vorticity

ACKNOWLEDGEMENTS

We are grateful to Paul-Antoine Libourel, Hugues Clamouze, Ashley Heers and Brandon Jackson for their help during the experiments. Thanks to Bieke Van Hooydonck and Anthony Herrel for the force platform used in Paris. Thanks to Camille Dégardin for her help with the illustrations. We also thank Peter Aerts and an anonymous reviewer for their helpful comments on an earlier version of the manuscript.

FUNDING

This research was supported by grants from the UMR 7179, l'Action Transversale du Muséum National d'Histoire Naturelle formes possibles, formes réalisées and from Ecole Doctorale Frontières du Vivant and Bettencourt-Schueller foundation fellowships as well as the National Science Foundation [grant nos IOS-0923606 and IOS-0919799].

REFERENCES

Abourachid, A. (1993). Mechanics of standing in birds: functional explanation of lameness problems in giant turkeys. *Br. Poult. Sci.* **34**, 887-898.

Abourachid, A., Hackert, R., Herbin, M., Libourel, P. A., Lambert, F., Gioanni, H., Provini, P., Blazevic, P. and Hugel, V. (2011). Bird terrestrial locomotion as revealed by 3D kinematics. *Zoology* **114**, 360-368.

Askew, G. N., Marsh, R. L. and Ellington, C. P. (2001). The mechanical power output of the flight muscles of blue-breasted quail (*Coturnix chinensis*) during take-off. *J. Exp. Biol.* **204**, 3601-3619.

Berg, A. M. and Biewener, A. A. (2010). Wing and body kinematics of takeoff and landing flight in the pigeon (*Columba livia*). *J. Exp. Biol.* **213**, 1651-1658.

Bonser, R. H. C. and Rayner, J. M. V. (1996). Measuring leg thrust forces in the common starling. *J. Exp. Biol.* **199**, 435-439.

Clark, J. and Alexander, R. M. (1975). Mechanics of running by quail (*Coturnix*). *J. Zool.* **176**, 87-113.

Crandell, K. E. and Tobalske, B. W. (2011). Aerodynamics of tip-reversal upstroke in a revolving pigeon wing. *J. Exp. Biol.* **214**, 1867-1873.

Dabiri, J. O. (2005). On the estimation of swimming and flying forces from wake measurements. *J. Exp. Biol.* **208**, 3519-3532.

Dial, K. P. (2003). Wing-assisted incline running and the evolution of flight. *Science* **299**, 402-404.

Dial, K. P. and Biewener, A. A. (1993). Pectoralis-muscle force and power output during different modes of flight in pigeons (*Columbia livia*). *J. Exp. Biol.* **176**, 31-54.

Dial, K. P., Jackson, B. E. and Segre, P. (2008). A fundamental avian wing-stroke provides a new perspective on the evolution of flight. *Nature* **451**, 985-989.

Dickinson, M. H., Lehmann, F. O. and Sane, S. P. (1999). Wing rotation and the aerodynamic basis of insect flight. *Science* **284**, 1954-1960.

Dickinson, M. H., Farley, C. T., Full, R. J., Koehl, M. A. R., Kram, R. and Lehman, S. (2000). How animals move: an integrative view. *Science* **288**, 100-106.

Doligalski, T. L., Smith, C. R. and Walker, J. D. A. (1994). Vortex interactions with walls. *Annu. Rev. Fluid Mech.* **26**, 573-616.

Earls, K. D. (2000). Kinematics and mechanics of ground take-off in the starling *Sturnis vulgaris* and the quail *Coturnix coturnix*. *J. Exp. Biol.* **203**, 725-739.

Ellington, C. P. (1984). The aerodynamics of hovering insect flight. 4. Aerodynamic mechanisms. *Philos. Trans. R. Soc. Lond. B* **305**, 79-113.

Garner, J. P., Taylor, G. K. and Thomas, A. L. R. (1999). On the origins of birds: the sequence of character acquisition in the evolution of avian flight. *Proc. R. Soc. B* **266**, 1259-1266.

Gatesy, S. M. and Dial, K. P. (1993). Tail muscle-activity patterns in walking and flying pigeons (*Columbia livia*). *J. Exp. Biol.* **176**, 55-76.

Gatesy, S. M. and Dial, K. P. (1996). Locomotor modules and the evolution of avian flight. *Evolution* **50**, 331-340.

Han, C. and Cho, J. (2005). Unsteady trailing vortex evolution behind a wing in ground effect. *J. Aircr.* **42**, 429-434.

Hartley, R. and Sturm, P. (1997). Triangulation. *Comput. Vis. Image Underst.* **68**, 146-157.

Heppner, F. H. and Anderson, J. G. T. (1985). Leg thrust important in flight take-off in pigeon. *J. Exp. Biol.* **114**, 285-288.

Jackson, B. E. and Dial, K. P. (2011). Scaling of mechanical power output during burst escape flight in the Corvidae. *J. Exp. Biol.* **214**, 452-461.

Norberg, R. A. and Norberg, U. M. (1971). Take-off and landing and flight speed during fishing flights of *Gavia stellata*. *Ornis Scandinavica* **2**, 55-67.

Ostrom, J. H. (1974). Archaeopteryx and the origin of flight. *Q. Rev. Biol.* **49**, 27-47.

Padian, K. (1987). *A Comparative Phylogenetic and Functional Approach to the Origin of Vertebrate Flight*. Cambridge, UK: Cambridge University Press.

Provini, P., Goupil, P., Hugel, V. and Abourachid, A. (2012). Walking, paddling, waddling: 3D kinematics of Anatidae locomotion (*Callonetta leucophrys*). *J. Exp. Zool.* **317**, 275-282.
R Development Core Team (2010). *R: A Language and Environment for Statistical Computing*. R Foundation for Statistical Computing, Vienna, Austria. Available at: http://www.R-project.org.
Ros, I. G., Bassman, L. C., Badger, M. A., Pierson, A. N. and Biewener, A. A. (2011). Pigeons steer like helicopters and generate down- and upstroke lift during low speed turns. *Proc. Natl. Acad. Sci. USA* **108**, 19990-19995.
Rüppell, G. (1975). *Bird Flight*, pp. 1-191. New York: Van Nostrand Reinhold.
Sane, S. P. (2003). The aerodynamics of insect flight. *J. Exp. Biol.* **206**, 4191-4208.
Simpson, S. F. (1983). The flight mechanism of the pigeon *Columbia livia* during take-off. *J. Zool.* **200**, 435-443.
Spedding, G. R. (1993). On the significance of unsteady effects in the aerodynamic performance of flying animals. *Contemp. Math.* **141**, 401-419.
Spedding, G. R., Rosén, M. and Hedenström, A. (2003). A family of vortex wakes generated by a thrush nightingale in free flight in a wind tunnel over its entire natural range of flight speeds. *J. Exp. Biol.* **206**, 2313-2344.
Tobalske, B. W. (2007). Biomechanics of bird flight. *J. Exp. Biol.* **210**, 3135-3146.
Tobalske, B. W. and Biewener, A. A. (2008). Contractile properties of the pigeon supracoracoideus during different modes of flight. *J. Exp. Biol.* **211**, 170-179.
Tobalske, B. W. and Dial, K. P. (2000). Effects of body size on take-off flight performance in the Phasianidae (Aves). *J. Exp. Biol.* **203**, 3319-3332.
Tobalske, B. W. and Dial, K. P. (2007). Aerodynamics of wing-assisted incline running in birds. *J. Exp. Biol.* **210**, 1742-1751.
Tobalske, B. W., Peacock, W. L. and Dial, K. P. (1999). Kinematics of flap-bounding flight in the zebra finch over a wide range of speeds. *J. Exp. Biol.* **202**, 1725-1739.
Tobalske, B. W., Hedrick, T. L. and Biewener, A. A. (2003). Wing kinematics of avian flight across speeds. *J. Avian Biol.* **34**, 177-184.
Tobalske, B. W., Altshuler, D. L. and Powers, D. R. (2004). Take-off mechanics in hummingbirds (Trochilidae). *J. Exp. Biol.* **207**, 1345-1352.
Vogel, S. (1994). *Life in Moving Fluids: the Physical Biology of Flow.* Princeton, NJ: Princeton University Press.
Warrick, D. R., Tobalske, B. W. and Powers, D. R. (2005). Aerodynamics of the hovering hummingbird. *Nature* **435**, 1094-1097.

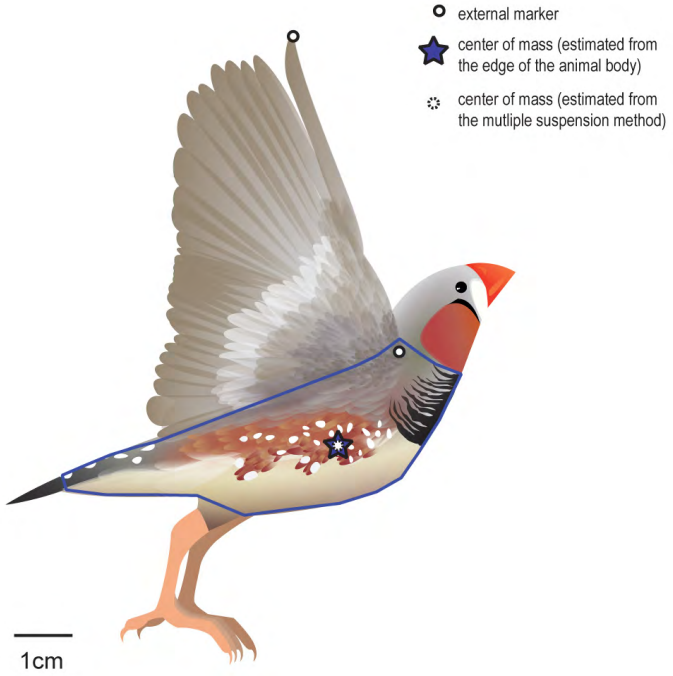

Fig. S1. Drawing of a zebra finch (*Taeniopygia guttata*) with the position of the digitized landmarks and the edge of the animal used to calculate the position of the geometric centre. The position of the centre of mass estimated using the multiple suspension method is represented by a circle.

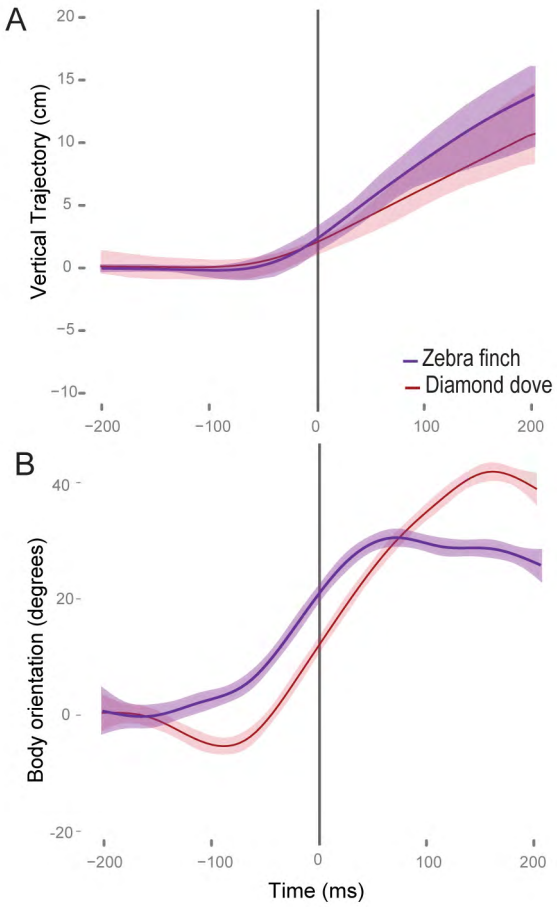

Fig. S2. (A) Vertical trajectory of the centre of mass over time in zebra finch (*Taeniopygia guttata*) (purple) and diamond dove (*Geopelia cuneata*) (pink). (B) Body orientation in zebra finch (purple) and diamond dove (pink). Time zero is at lift-off.